

# The Cross-Bridge Dynamics during Ventricular Contraction Predicted by Coupling the Cardiac Cell Model with a Circulation Model

Eun Bo SHIM<sup>1,2</sup>, Akira AMANO<sup>1,4</sup>, Takayuki TAKAHATA<sup>1,5</sup>, Takao SHIMAYOSHI<sup>1,4,6</sup>, and Akinori NOMA<sup>1,3</sup>

<sup>1</sup>Cell/Biodynamics Simulation Project, Kyoto University, Kyoto, Japan; <sup>2</sup>Department of Mechanical & Biomedical Engineering, Kangwon National University, Hyoja-dong, Chuncheon, Kangwon 200-701, Korea; <sup>3</sup>Department of Physiology and Biophysics, Graduate School of Medicine, Department of Physiology, Kyoto University, Kyoto, Japan; <sup>4</sup>Graduate School of Informatics, Kyoto University, Kyoto, Japan; <sup>5</sup>The Central Research Laboratories of Sysmex Corporation, 4-4-4 Takatsukadai, Nishi-ku, Kobe, 651-2271 Japan; and <sup>6</sup>ASTEM Research Institute of Kyoto, Kyoto, Japan

**Abstract:** The force-velocity (F-V) relationship of filament sliding is traditionally used to define the inotropic condition of striated muscles. A simple circulation model combined with the Laplace heart was developed to get a deeper insight into the relationship between the F-V characteristics and the cardiac ventricular inotropy. The circulation model consists of a preload and an afterload compartments. The linear F-V relationship for filament sliding in the NL model (Negrone and Lascano 1996) was replaced by the exponential F-V relation observed by Piazzesi *et al.* (2002). We also modified the NL model to a hybrid model to benefit from the Ca<sup>2+</sup> cooperativity described by the Robinson model (Robinson *et al.* 2002). The model was validated by determining the diastolic ventricular pressure-volume relationship of

the Laplace heart and the F-V relation of the new hybrid model. The computed parameters of the cardiac cycle agreed well with the physiological data. Computational results showed that the cross-bridge elongation ( $h$  in the NL model) temporally undershot the equilibrium  $h_c$  during the ejection period and overshot it during the rapid refilling phase. Thereby the time course of ejection and refilling was retarded. In a simulation where the velocity of the mobile myosin head ( $dX/dt$ ) was varied, the systolic peak pressure of the ventricle varied from a minimum value at  $dX/dt = 0$  to a saturating value obtained with a constant  $h_c$ , providing *in silico* evidence for a functional impact of the cross-bridge sliding rate on the ventricular inotropy.

**Key words:** force-velocity relationship, cardiac ventricular cell model, circulation.

The velocity of myofilament sliding is maximum in the absence of external load and decreases exponentially with increasing external load [1]. This force-velocity (F-V) relationship, together with the sarcomere length-force (L-F) relationship, is a classic measure in the evaluation of muscle inotropy. The velocity of muscle shortening is influenced by positive inotropic agents such as  $\beta$ -adrenergic agonists, external Ca<sup>2+</sup> concentration ( $[Ca^{2+}]_o$ ), and the initial muscle length. Despite substantial progress in understanding the mechanisms that control heart inotropy, the dynamic relationship between the F-V relation of myofilaments and the blood-pumping of the ventricle is still not fully understood. This is because physiological cardiac contraction is neither isometric nor isotonic. Arguably, computer modeling of cardiac myocyte contraction can provide a tool to predict how the cardiac pump function is affected by modifying the F-V relation. In 1999, Negrone and Lascano examined the contribution of the cross-bridge dynamics to the pressure development in the ven-

tricle by calculating the time course of the cross-bridge elongation during a flow-clamped condition at a constant concentration of the extracellular Ca<sup>2+</sup>  $[Ca^{2+}]_o$  [2]. They found that the average cross-bridge elongation ( $h$ ) decreased during the descending volume ramp, and thus the force of contraction during the ejection period was directly reduced by the decrease in  $h$ . However, one of the main limitations of the NL model [3] is that the F-V relation for the filament sliding is assumed to be linear. This assumption is unrealistic, since the experiment by Piazzesi *et al.* revealed that it varies exponentially in the skeletal muscle [1]. We have therefore introduced an exponential F-V relation based on the experimental observation. Moreover, no positive cooperativity is represented by the NL model in the  $[Ca^{2+}]$ -force relationship, which is critical in determining the time course of contraction. Thus it was necessary to develop a new contraction model by combining the NL model and the Robinson model [4] to reproduce the apparent cooperativity in the Ca<sup>2+</sup> activation. The hybrid

Received on Jun 7, 2007; accepted on Oct 3, 2007; released online on Oct 10, 2007; doi:10.2170/physiolsci.RP006007

Correspondence should be addressed to: Akinori Noma, Department of Physiology and Biophysics, Graduate School of Medicine, Kyoto University, Kyoto, Japan. Phone: +81-75-753-4352, Fax: +81-75-753-4349, E-mail: noma@card.med.kyoto-u.ac.jp

contraction model was then coupled with the cellular excitation model of human cardiac myocytes [5]. Eventually, the Laplace heart driven by cell contraction [6] was implemented to simulate the interaction between the F-V relationship and the cardiac pumping activity. The model demonstrates that the magnitude of  $h$  varies during the ventricular ejection or refilling period, as suggested by Negroni and Lascano [3], and that the peak ventricular pressure and the time course of ventricular contraction change according to the variation of the sliding rate of the myosin head along the actin filament.

**METHODS**

Ordinary differential equations were integrated using the Euler method with a time step of 0.025 ms.

**The biological Laplace heart combined with preload and afterload.** We developed an integrative mathematical model of blood circulation, including the Laplace heart, a simple preload, and an afterload, as shown in Fig. 1. The preload was characterized by a constant pulmonary venous pressure ( $P_{pv}$ ) and the pressure of the left atrium ( $P_{la}$ ). The afterload was characterized by the aortic pressure ( $P_{ao}$ ), the arterial pressure ( $P_a$ ), and a constant systemic venous pressure ( $P_v$ ). The volume ( $V$ ) change over time  $t$  can be described by Eq. 1 for each compartment of the left atrium, left ventricle, aorta, and arteries.

$$\frac{dV}{dt} = Q_{in} - Q_{out} \tag{1}$$

where  $Q_{in}$  is the inflow of blood into the compartment, and  $Q_{out}$  is the outflow. The flow ( $Q_{ab}$ ) between compartments a and b is given by

$$Q_{ab} = (P_a - P_b)/R_{ab} \tag{2}$$

$$\text{and } P = V/C, \tag{3}$$

where  $R_{ab}$  is the resistance between compartments a and b, and  $C$  denotes the compliance of the compartment. The

functions of the mitral and aortic valves were represented by the two “diodes” positioned next to the atrium and ventricle, respectively. The magnitudes of parameters were slightly modified from the original values in the literature, as shown in Table 1.

For the left ventricle, the Laplace heart pressure ( $P_{lv}$ ) was computed as

$$P_{lv} = \frac{2T}{r_{lv}}, \tag{4}$$

where  $T$  is the wall tension generated by the contracting units and  $r$  the radius of the Laplace heart.  $T$  is determined

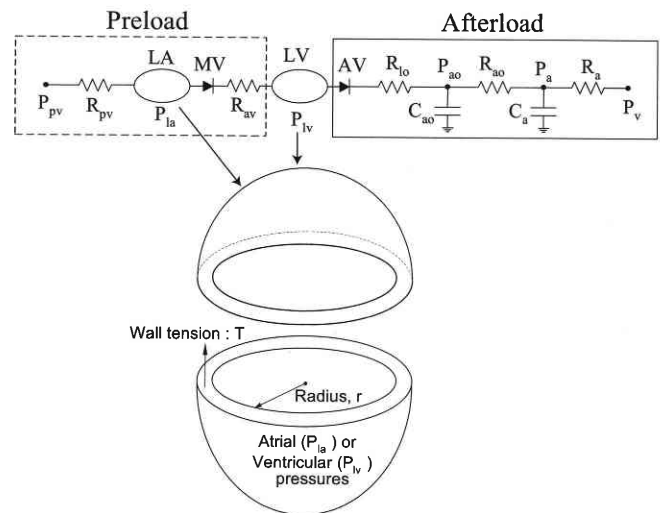


**Fig. 1.** Schema of the integrated model of the cell-cardiovascular system.  $R$  denotes the blood flow resistance (resistance) and  $C$  the vessel compliance (capacitance). The subscripts lo, ao, a, v, and pv indicate the left ventricle outlet, aorta, arteries, veins, and pulmonary veins, respectively. The cardiac valves ensuring the unidirectional blood flow are denoted by diodes (black triangles). Atrium and ventricle are represented using the thin-walled spherical model. The ventricular pressure and the wall tension generated by the myocytes are correlated by Laplace’s law. For the atrium, the same approach was applied.

**Table 1.** Summary of the constants for the cardiovascular system model.

Present model		Reference
$R_{av} = 0.0025$ PRU (=mmHg·s/ml)	Heldt <i>et al.</i> [18]	0.0025 PRU
$R_{pv} = 0.006$ PRU	Heldt <i>et al.</i> [18]	0.006 PRU
$R_{lo} = 0.004$ PRU	Heldt <i>et al.</i> [18]	0.004 PRU
$R_{ao} = 0.03$ PRU	Ursino [19]	0.03 PRU
$C_{ao} = 0.3$ ml/mmHg	Ursino [19]	0.03 ml/mmHg
$R_a = 1.0$ PRU	Heldt <i>et al.</i> [18]	1.0 PRU
$C_a = 1.7$ ml/mmHg	Heldt <i>et al.</i> [18]	0.03 ml/mmHg
$P_v = 4$ mmHg	Heldt <i>et al.</i> [18]	4 mmHg
$P_{pv} = 12$ mmHg	Heldt <i>et al.</i> [18]	8 mmHg
Unstressed volume of ventricle = 100 ml	Heldt <i>et al.</i> [18]	90–100 ml
Unstressed volume of atrium = 25 ml	Heldt <i>et al.</i> [18]	25 ml

The unstressed volume in the present model was defined by  $F_b = 0$  and  $L = L_0$ .

**Table 2.** Comparison of the simulated results with a set of standard measurements in the literature [18].

Variables	Normal range	Average	Present simulation
LV pressure			
Systole	90–140 mm Hg	121 mm Hg	120.5 mm Hg
End-diastole	4–12 mm Hg	9 mm Hg	13.5 mm Hg
Arterial pressure			
Systole	90–140 mm Hg	118 mm Hg	100 mm Hg
Diastole	60–90 mm Hg	80 mm Hg	71 mm Hg
Cardiac output	4,700–7,100 ml/min	4,800 ml/min	4,891 ml/min
Stroke volume	51–110 ml	69 ml	68 ml (EF = 0.54)

by multiplying  $F$  across a unit area of muscle cut end with a constant muscle thickness at rest (8 mm for LV based on published data [7]). The ventricular volume obtained from Eq. 1 was converted to  $r_{LV}$ . The half-sarcomere length ( $L$ ) of the myocyte in the cell model was then computed by  $2\pi r_{LV}/N$ , where  $N$  is the total number of half-sarcomere along the circumference of the Laplace ventricle. The force of the contracting unit was calculated using this new value of  $L$  in the next time step of integration. For the atrium, the same approach as for the left ventricle was applied to compute the half-sarcomere length and the pressure in the thin-walled left atrium with the Laplace heart shape. All parameters related to the systemic circulation model are presented in Table 2, as measured when the cyclic changes in the ventricular pressure reached a steady state.

The wall tension of the Laplace heart was calculated by assuming a “numerous number” of the contraction units (NL model) uniformly distributed on the surface of the shell. It is assumed that the contraction units are distributed homogeneously in all directions on the shell of the

Laplace heart, allowing the wall tension over the entire wall of the sphere to be uniform. All contracting units were driven synchronously by a common  $Ca^{2+}$  transient, which was computed using the electrophysiological model of the human atrial and ventricular myocytes proposed by Nygren *et al.* (Nygren model) [8] and tenTusscher *et al.* (TNNP model) [5], respectively. The parameters of the TNNP model were modified to obtain a more realistic  $Ca^{2+}$  transient; the parameter  $arel$  ( $=16.464$  mM/s) was decreased to 4.0 mM/s, and  $crel$  ( $=8.232$  mM/s) was decreased to 0.8232 mM/s to reduce the peak amplitude; the parameter  $\tau_g$  ( $=2.0$  ms) was increased to 30.0 ms to delay the peak time, and the parameter  $V_{maxup}$  ( $=0.000425$  mM/ms) was increased to 0.0007 mM/ms to obtain a faster decay of the  $Ca^{2+}$  transient. To simplify the analysis, the elastic element in the series with the muscle unit was not included except in the examination of the F-V relation in Figs. 3 and 4, even though it transiently influences the cross-bridge elongation during the rising phase of the contraction (Fig. 7 in Negroni and Lascano [2]). In the present study, we call this hypothetical heart the “biological

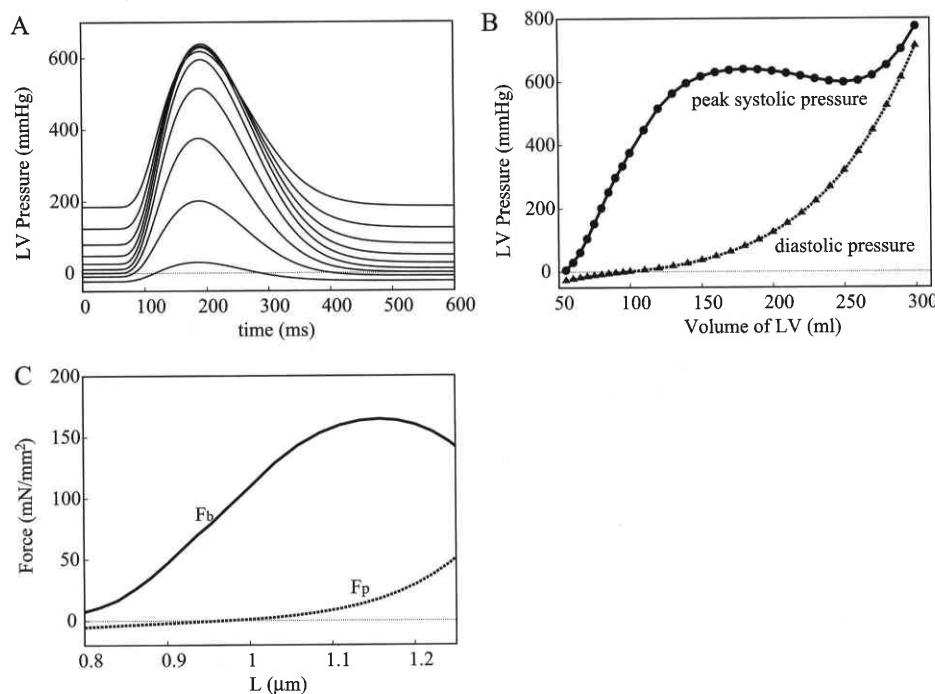


**Fig. 2.** Reconstruction of the volume-force relations. The ventricular cavity was isolated from the preload and afterload in Fig. 1, and the isovolumic contraction was activated at 1 Hz with varying resting volume. (A) original traces; (B) pressure measured at the peak of the developed pressure (circles) and pressure measured at the diastole (triangles); (C) isometric contraction of the ventricular cell model;  $F_b$  and  $F_p$  as defined by Eqs. A18 and A19 in the APPENDIX.

Laplace heart" to distinguish it from the conventional ventricular compartment driven by time-varying capacitance.

The development of the hybrid contraction model by combining the NL model, corrected for the F-V relationship [1] with the Robinson model, is described in the APPENDIX.

## RESULTS

### Reconstruction of the volume-pressure relationship using the proposed model

The analysis of cross-bridge dynamics during the ventricular contraction is critically dependent on the validity of the cross-bridge model. We tested the hybrid contraction model for its mechanical characteristics by constructing the volume-pressure relationship and the F-V relationship. In a simulation of the Frank [9] experiment (see also Ref. [10]), the diastolic volume ( $V_d$ ) of the biological Laplace ventricle was fixed after its disconnection from the preload and afterload, and the time course of the developed tension was recorded under the condition of isovolumic contraction. With increasing  $V_d$ , the diastolic pressure increased exponentially as shown in Fig. 2, A and B, reflecting mainly the L-F relationship of the parallel elastic component ( $F_p$ ) of the NL model. The contracting units on the shell of the biological Laplace ventricle were activated by the  $Ca^{2+}$  transient generated by the ventricular cell model, which was stimulated at 50 ms on the time scale in Fig. 2A. The isovolumic systolic pressure peaked at approximately 200 ms. In the volume-pressure relation in Fig. 2B, the systolic pressure peaked at a volume of 160 ml and then declined with a further increase in volume until the steep increase in diastolic pressure caused an additional rising limb of the relationship. These relationships are similar to the classic experiment of Frank [9] in frog hearts. In the present model, the diastolic pressure is determined by the  $F_p$ -L relationship of the parallel elastic component (Eq. A19, APPENDIX), and the peak systolic pressure is determined by the force  $F_b$ -L relationship of the cross-bridge (Eq. A18) shown in Fig. 2C. We conclude that the findings in Fig. 2, A and B, validate the mechanical characteristics of the hybrid model.

**The F-V relationship of the hybrid model.** We examined the hybrid model in the isotonic contraction for its response to step changes in the load by deriving the analytical solution of the hybrid model, which is described in the APPENDIX.  $[Ca^{2+}]_i$  was assumed to be constant. The force equilibrium condition of the hybrid model can be written as follows:

$$K_b(L - X) + K_p \cdot f_p(L) = F_{ext} \quad (5)$$

where  $L$  and  $X$  represent the half-sarcomere length and the inextensible length of the half-sarcomere, respectively.  $K_b$  denotes the active force coefficient and is given in the NL model (see Scheme A1 in the APPENDIX) as,

$$K_b = A \cdot ([TCa^*] + [T^*]) \quad (6)$$

$K_p$  represents passive force coefficients ( $K_{PE}$  and  $K_{PL}$  in Eq. A19), and  $f_p(L)$  represents the dependency of  $F_p$  on  $L$ . The velocity of half-sarcomere shortening,  $dL/dt$ , is given as

$$\frac{dL}{dt} = \frac{K_b \frac{dX}{dt} - (L - X) \frac{dK_b}{dt}}{K_b + K_p \frac{df_p(L)}{dL}} \quad (7)$$

Thus the measurement of  $dL/dt$  can give the value  $dX/dt$  when the conditions of  $dK_b/dt = 0$  and  $K_p = 0$  are met.

$$\frac{dL}{dt} = \frac{dX}{dt} \quad (8)$$

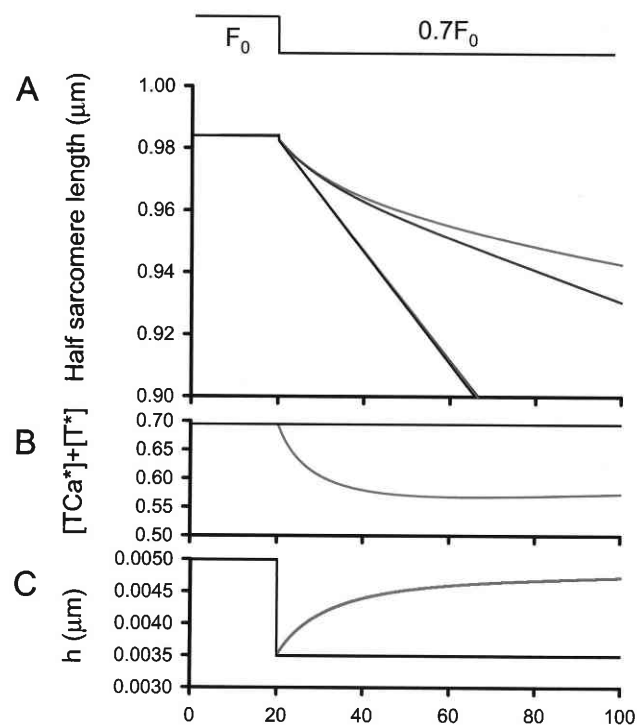


**Fig. 3.** Effects of  $Q_d$ ,  $F_p$ , and  $S$  function on the measurement of  $dL/dt$  in the force clamp experiment. A steady-state condition of the hybrid model was established with an initial set of parameters:  $[Ca^{2+}] = 2 \mu M$ , the half-sarcomere length  $L = 0.983 \mu m$ , and the length of the series elastic component  $L_{sm} = 0.067 \mu m$ .  $F_{ext}$  was  $368.5 \text{ mN/cm}^2$  in the steady state, then decreased by 30% at time 20 ms as shown in the graph on the top. The simulation was conducted under four conditions: (1) The values of  $Q_d$ ,  $F_p$ , and  $S$  function were all fixed to the values obtained at the end of the conditioning period and kept constant during the test period while  $0.7 F_{ext}$  was being applied; (2) Time-dependent changes in  $F_p$  were included; (3) time-dependent changes in  $Q_d$  and  $F_p$  were included; and (4) time-dependent changes in  $Q_d$ ,  $F_p$ , and  $S$  function were included. The simulation (1) yielded a linear change of  $L$ , and  $[TCa^*] + [T^*]$  and  $h$  both remained constant (black curves in A, B, and C). The addition of the time-dependent change of  $Q_d$  in simulation (3) induced the marked changes in all three parameters, but the effects of  $F_p$  and  $S$  function in simulation (2) and (4) were much smaller.

In experiments, the parallel elastic component  $K_p$  could be minimized by using a single fiber of the skeletal muscle, which is free from the extracellular connective tissue, as in the experiment of Piazzesi *et al.* [1]. It is difficult to satisfy the condition of  $dK_p/dt = 0$ , however, because the sum ( $[TCa^*] + [T^*]$ ) in Eq. 6 changes with time through the flux ( $Q_d$ ) of the original NL model (Scheme 1A, APPENDIX).

$$Q_{d1} = Y_d \cdot (dX/dt)^2 \cdot [TCa^*]$$

$$Q_{d2} = Y_d \cdot (dX/dt)^2 \cdot [T^*]$$

(9)

Therefore time-dependent changes in  $dK_p/dt$ , or, in other words, time-dependent changes in the number of cross-bridges (proportional to  $[TCa^*] + [T^*]$ ), cannot be neglected even in the single fiber experiments of the skeletal muscle. We assume that the property obtained in the skeletal muscle is applicable to the cardiac muscle, where a systematic measurement of developed tension in isolated myocytes is difficult.

We examined the influence of  $dK_p/dt$  on the measurements of the force-velocity relation by simulating the F-V experiment using the presented hybrid model (Fig. 3). A steady-state condition was established under isometric contraction ( $L = 0.983 \mu\text{m}$ ,  $[Ca^{2+}] = 2 \mu\text{M}$ ), and  $F_{\text{ext}}$  was defined as  $F_0$  ( $= 368.5 \text{ mN/mm}^2$ ). At 20 ms,  $F_{\text{ext}}$  was decreased to 70% as shown on the top of the graph in Fig. 3. As a reference, a simple condition was calculated by excluding the time-dependent changes in ( $[TCa^*] + [T^*]$ ). That means the values of  $Q_d$ ,  $F_p$ , and the  $S$  function (Eq. A15) were fixed during the test step to the respective values obtained at the end of the conditioning period. After the step change in  $F_{\text{ext}}$ , the half-sarcomere length  $L$  decreased linearly with a constant  $dL/dt$ , which was equal to  $dX/dt$  defined by Eq. A17 (black line in Fig. 3A). Under this condition, both the magnitude of ( $[TCa^*] + [T^*]$ ) (black line in B) and the cross-bridge elongation  $h$  (black line in C) remained constant. When the time-dependent change in  $F_p$  was included, the linear time course of the half-sarcomere shortening was only slightly modified, as shown by the green curve in Fig. 3A. A marked modification of the time course was observed when  $Q_d$  flux was activated. The  $dL/dt$  progressively decreased to a new steady value as shown in Fig. 3A (blue curve). Finally, when the time-dependent change in the  $S$  function on top of the  $Q_d$  flux was added, a further delay was observed in  $dL/dt$  (the red curve in A). It is obvious that the deceleration in  $dL/dt$  is caused by an increase of load applied to individual cross bridges, as indicated by the time-dependent decreases in ( $[TCa^*] + [T^*]$ ) (red curve in B), which indicates the decrease in the number of cross bridges, and accordingly  $h$  increased with time after the step change in  $F_{\text{ext}}$  (upward deflection in the red curve in Fig. 3C).

In experimental studies, the initial slope  $dL/dt$  immediately after the  $F_{\text{ext}}$  jump is usually measured as an index of

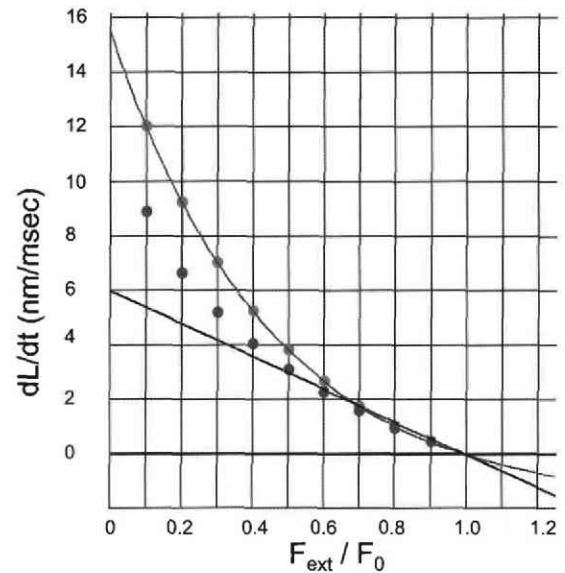


**Fig. 4.** The  $dL/dt$  measured immediately after the jump in  $F_{\text{ext}}$  in the simulation described in Fig. 3. The red points correspond to the measurements of  $dL/dt$  under condition (1) and are equal to  $dX/dt$  (blue curve) given by Eq. A17. The blue points are those obtained under condition (4). The straight black line depicts  $dX/dt$  given by the original NL model (Eq. A16). On the abscissa,  $F_0$  is  $F_{\text{ext}}$  at the end of the conditioning period.

$dX/dt$ . In the present simulation, the  $dL/dt$  was measured over a time window of 1 msec in duration and starting 0.1 ms after the force jump by varying  $F_{\text{ext}}/F_0$  over the range from 0.1 to 0.9 as indicated on the abscissa. The measurements for the simplest and the full cases are shown in Fig. 4. The value of  $dL/dt$  (red circles) was equal to the theoretical  $dX/dt$  (blue curve) when the values of  $Q_d$ ,  $F_p$ , and the  $S$  function were fixed to the values obtained at the end of the conditioning period. When the time-dependent changes in all of  $Q_d$ ,  $F_p$ , and the  $S$  function were reintroduced, the initial slope ( $dL/dt$ , blue circles) was clearly decreased. These simulation results in the isotonic shortening experiment indicate that the rate  $dL/dt$  approximates  $dX/dt$  only at the onset of applying a new  $F_{\text{ext}}$ , even though the values are underestimated. This behavior of the hybrid model is in good agreement with the assumption used in the experimental studies that the  $dX/dt$  can be approximated by the initial  $dL/dt$ . We conclude that the present hybrid model of contraction is well validated.

**From single cell excitation-contraction to blood pressure in the circulation model.** In Fig. 5, the activities of the biological Laplace heart with corresponding changes in the systemic parameters are demonstrated for different construction levels, from the single cell to the whole heart. The heart was stimulated in an interval of 833 ms with a delay of 120 ms between the atrial and ventricular stimulations. The action potential of a TNNP model showed the characteristic shape described in human ventricular cells close to the endothelium with a resting potential of  $-85.9$

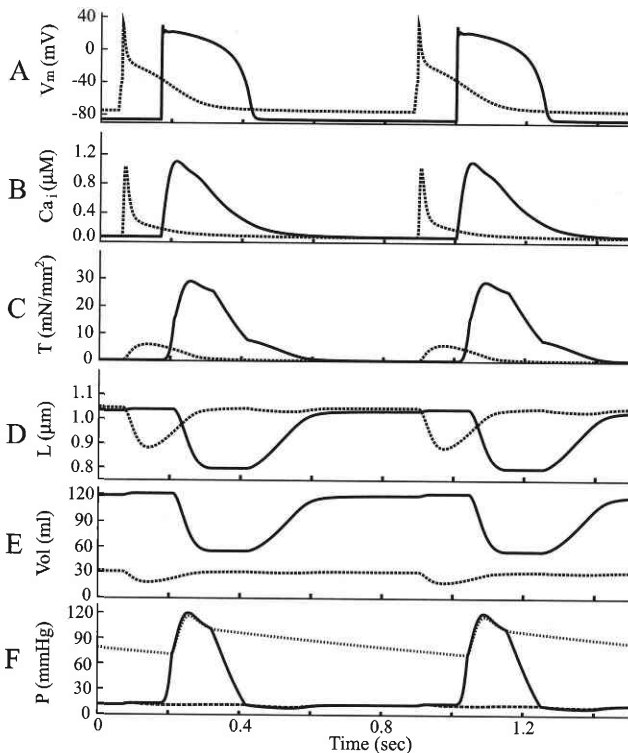


**Fig. 5.** Computed results for the sequential events in the cell-system model. **(A)** Action potentials, **(B)**  $\text{Ca}^{2+}$  transients, **(C)** developed force, **(D)** half-sarcomere length, **(E)** volume of the ventricle and atrium, **(F)** LV (continuous line), LA (dashed line), and aortic pressure (dotted line).

mV, whereas a sharp spike followed by a linear repolarization phase is typical for the atrial action potential (Fig. 5A). The  $\text{Ca}^{2+}$  transient (Fig. 5B), which was triggered by the action potential, developed a wall tension ( $T$ ), as shown in Fig. 5C. The time course of  $T$  is largely modified by the blood flow if compared with the pressure profile in the isovolumic contraction of the ventricle shown in Fig. 2A. The force of the contraction in the atrium is approximately a fifth of the ventricle. As in the normal heart, the contraction of the atrium caused only a minor increase in the ventricular volume  $V_{\text{lv}}$ . The half-sarcomere length in Fig. 2D decreased up to  $\sim 0.8 \mu\text{m}$  during systolic period, which indicates that the L-F relationship shown in Fig. 2C is the major determinant for limiting the  $L$  shortening. The contour of both,  $V_{\text{lv}}$  (Fig. 5E) and the blood pressure in the afterload (Fig. 5F), is determined by the balance between the inflow and the outflow for each compartment. The ejection fraction in the present model is 0.54. The parameters of the circulation listed in Table 2 are in good agreement with the standard values.

**Dynamic changes of the cross-bridge elongation during the heart cycle.** Figure 6 demonstrates the time-varying probability of the cross bridge attached to the thin filament ( $[\text{TCa}^*] + [\text{T}^*]$ ),  $h$ ,  $L$ , and  $F_b$  for one cardiac cycle. Surprisingly, the value of  $h$  was not constant during the cardiac cycle; the value  $h$  decreased temporarily during

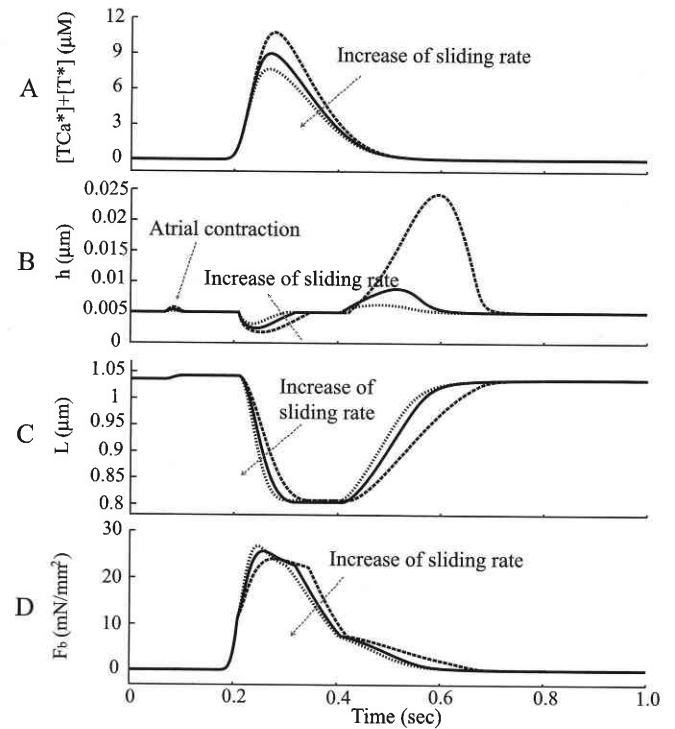


**Fig. 6.** Effects of changing the sliding rate  $B_{\text{eff}}$  on the relative number of the attached cross bridges **(A)**; the cross-bridge elongation  $h$ , **(B)**; the shortening of the half-sarcomere length,  $L$ , **(C)**; and cross-bridge force,  $F_b$ , **(D)**. The cross-bridge sliding rate of the dotted line was determined with  $B_{\text{eff}} = -0.944$ ; the continuous line with  $B_{\text{eff}} = -1.887$ ; and the dashed line with  $B_{\text{eff}} = -3.77 \mu\text{m/ms}$ .

the ejection period and increased during the refilling period. This means that during shortening, relative motion between the thin and thick filaments ( $dL/dt$ ) reduced the average cross-bridge elongation ( $h$ ). Simultaneously, the myosin head moves to restore the equilibrium length ( $h_c = 0.005 \mu\text{m}$ ) of the cross bridge. Clearly, the velocity  $dL/dt$  is faster than  $dX/dt$  during the initial half of the fast ejection period and caused the decrease in  $h$ . This relationship is even more clearly demonstrated when simulating the same protocol after varying the sliding rate  $dX/dt$ , which is given by Eq. A17,

$$dX/dt (\mu\text{m}\cdot\text{ms}^{-1}) = B_{\text{eff}} \left( e^{\frac{h_c - h}{0.00225}} - 1 \right)$$

where  $B_{\text{eff}}$  is a magnitude factor. With smaller  $B_{\text{eff}}$  ( $= -0.944 \mu\text{m/s}$ ), the depth of sag below  $h_c$  is larger than with the standard  $B_{\text{eff}}$  ( $= -1.887 \mu\text{m/s}$ ), and the larger  $B_{\text{eff}}$  ( $= -3.77 \mu\text{m/s}$ ) caused a shallow sag. Since  $F_b$  is proportional to  $h$  (Eq. A18),

$$F_b = A \cdot S \cdot ([\text{TCa}^*] + [\text{T}^*]) \cdot h$$

the temporal shortening of  $h$  by 38%, 52%, and 65% of  $h_c$  in Fig. 6B depressed the force development and prolonged the ejection period. During the refilling period,  $h$  was temporarily elongated and thus slightly delayed the

refilling time course. However, the extent of  $h$  elongation is disputable because it is merely suggested by extrapolating the  $dX/dt-h$  relationship (in Fig. 4) to the range of  $h > h_c$ , which has not been tested in experiments. It should be noted that the restriction of peak  $F_b$  in Fig. 6 is also caused by the progressive decrease in  $F_b$  with a shortening of  $L$  according to the L-F curve (Fig. 2C).

In Fig. 7, the value of  $B_{\text{eff}}$  was systematically changed, and the peak  $P_{\text{lv}}$  was plotted against  $B_{\text{eff}}$ . It is evident that peak  $P_{\text{lv}}$  is depressed to a larger extent with a decreasing sliding rate. The number of cross bridges (proportional to  $[TCa^{*}] + [T^{*}]$ ) decreased with increasing sliding rate (Fig. 6A), and thereby the decrease of  $F_b$  was partially compensated. The asymptotic value of  $P_{\text{lv}}$  toward the larger (more negative)  $B_{\text{eff}}$  is obtained when  $h$  remains constant ( $=h_c$ ). It is interesting that the standard value of  $B_{\text{eff}}$  is within the dynamic range of the relationship, thereby enabling an adjustment of the muscle inotropic condition through various kinds of physiological regulations of the myosin ATPase.

## DISCUSSION

In the present study a new contraction model was developed that satisfactorily reconstructed the high cooperativity in the  $Ca^{2+}$ -activation of contraction, the exponential F-V relationship, and the L-F relationship. Using the new contraction model, we confirmed the model prediction of Negroni and Lascano [2] that the average cross-bridge elongation is transiently decreased during the ejection period in the canine left ventricle, whereby the developed pressure is decreased by 20–30% if compared with the isovolumic contraction. Thus the ejecting pressure of the ventricle depends not only on the sarcomere length, but also on the cross-bridge elongation. We found that the same mechanism could be observed when the biological Laplace heart based on the human atrial and ventricular cell models was combined with a simple preload and afterload to simulate the physiological ejection pattern as well as the aortic pressure changes. This simulational condition is much more realistic if compared with that in the NL study [2], where a volume ramp was imposed on the ventricular model, which was triggered by a hypothetical  $Ca^{2+}$  transient or tetanized with a constant  $Ca^{2+}$  and isolated from the pre- and afterloads. In this study the relationship between the sliding rate and the peak systolic pressure was newly examined systematically, calculating the ventricular pressure by varying the sliding rate in Figs. 6 and 7.

### Physiological relevance

The dynamics of the cross bridge consist of a cycle of four sequential conformations [11]; a detached cross bridge, an attached cross bridge, an attached cross bridge storing developed force in the elastic component, and a

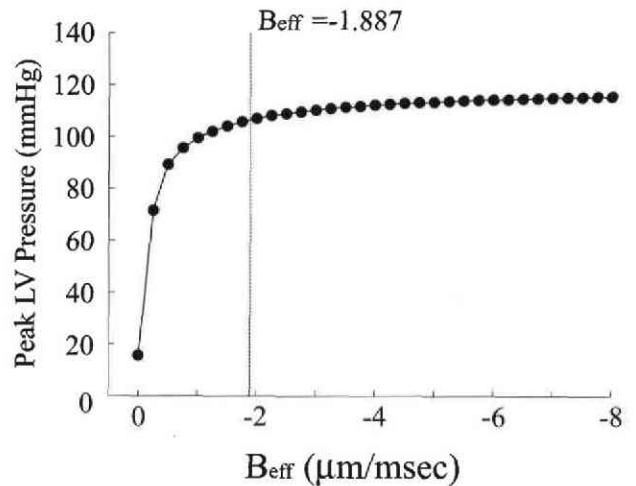


Fig. 7. Dependence of the peak LV pressure on the cross-bridge sliding rate  $B_{\text{eff}}$ . The  $B_{\text{eff}}$  of  $-1.887 \mu\text{m/ms}$  is the standard value in the hybrid model.

cross bridge rotated and translated so the filaments slide in relation to one another. Although this individual cycle might produce a stepwise movement of the myosin head along the thin filament, the average of asynchronous movements of a numerous number of cross-bridges within one myocyte can be described by a continuous function defined by both  $B_{\text{eff}}$  and average cross-bridge elongation  $h$ , as described in the NL model [3]. In the present study, we investigated the effects of varying sliding rate  $B_{\text{eff}}$  of the myosin head on heart mechanics, using a new cell system model to encompass cells and the pre- and afterloads. It is indicated that the peak systolic pressure in the ventricle is influenced in a dynamic manner when varying the value of  $B_{\text{eff}}$  in the hybrid model (Fig. 7). The delayed movement supported by smaller  $B_{\text{eff}}$  of the cross bridge on the thin filament is able to sustain force or pressure for a longer period of contraction at the expense of the peak tension. This maintenance of compromised pressure for longer periods with a given time course development of  $F_b$  in myocytes is favorable for pumping viscous blood from the heart to the compliant afterload. At the end systole, the value of  $h$  shows a rebound over the equilibrium elongation  $h_c$  in the same way as partly indicated in Fig. 11B of Negroni and Lascano [2].

### Relevance of the biological Laplace heart system

The relationship between the peak ventricular pressure and the sliding rate  $B_{\text{eff}}$  in Fig. 7 is determined largely by the bidirectional interaction between the mechanical part of the hybrid model and the dynamics of the Laplace heart. Therefore in the present study we first validated the hybrid model by reconstructing the ventricular pressure-volume relationship (Fig. 2) and the F-V relationship (Figs. 3 and 4). We also confirmed that the parameters of the circulation are in good agreement with estimated val-

ues between those of the simplified model and the experimental values (Table 2). Thus we believe that the presented biological Laplace heart combined with simple pre- and afterload models is appropriate for the simulation of the heart dynamics with varying cross-bridge kinetics.

In a separate series of simulations (not shown), we confirmed that the sag and overshoot of  $h$  around  $h_c$  also occurs in the smaller biological Laplace heart of the guinea pig during rapid ejection and refilling phases. This notion can be proved in an analytical way as follows:

The sphere-shaped volume ( $V$ ) of radius  $r$  equals

$$V = 4 \pi r^3 / 3 \quad (10)$$

Therefore

$$r = (3/4 \pi)^{1/3} V^{1/3} \quad (11)$$

For an end systolic volume of 40%  $V$  (the standard ejection fraction = 0.6), the radius  $r_{0.4}$  is

$$r_{0.4} = (3/4 \pi)^{1/3} 0.4^{1/3} V^{1/3} \quad (12)$$

Thus the ratio of the radius before and after the contraction is independent of the size of the Laplace heart.

$$r_{0.4}/r = 0.4^{1/3} = 0.736 \quad (13)$$

Since  $L$  is proportional to  $r$ , the extent of the shortening of  $L$  is also independent of the heart size.

$$L = 2\pi r/N \quad (14)$$

If large and small hearts have a common ejection period and a common ejection fraction, the velocity of the  $L$  shortening is equal for both hearts. If a smaller heart has a shorter ejection period, as is true in reality, the rate of  $L$  shortening will be faster in a small animal than in a large animal. Thus the effect depicted in Fig. 6 is expected to be even more prominent in a smaller heart provided a given value of  $B_{\text{eff}}$ . We therefore believe that the peak pressure- $B_{\text{eff}}$  relationship in Fig. 6 also holds for the small hearts of experimental animals.

### Limitations of the present study

The heart has a complex muscle layer exhibiting fiber anisotropy and heterogeneous muscle thickness. Also, different parts of the ventricles are activated with different timing. In our study, the ventricle is assumed to be a thin-walled Laplace heart to reduce the complexity of the coupled cell-circulation hemodynamics method. Thus the degree of sag or overshoot of  $h$  for the real heart may be different for different cells in different layers of the muscle.

In the real heart, the compliant ends of the muscle, which we did not include in the model, may also influence the relationship between the peak pressure- $B_{\text{eff}}$  relationship. The models for human atrial and ventricular cells are based on rather limited experimental data. Furthermore, the theory of nearest-neighbor cooperative influences was developed for the skeletal muscle rather than for the cardi-

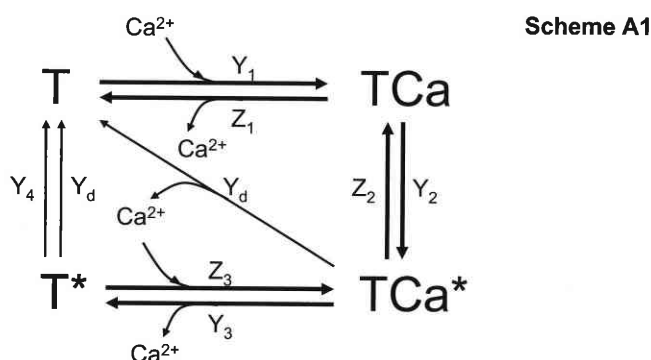
ac muscle [4]. It is expected that more complete human cell models will become available.

## APPENDIX

# A new cardiac contraction model based on an NL model and a Robinson model

by Takayuki TAKAHATA, Takao SHIMAYOSHI, Akira AMANO, Eun Bo SHIM, and Akinori NOMA

The cross-bridge dynamics in the Negroni and Lascano (NL) model [2, 3] are described by a four-state reaction scheme consisting of free troponin (T),  $\text{Ca}^{2+}$ -bound troponin (TCa),  $\text{Ca}^{2+}$ -bound troponin with attached cross bridge (TCa\*), and troponin with attached cross bridges (T\*), as shown in Schema A1.



$$d[\text{TCa}]/dt = Y_1 [\text{T}] + Z_2 [\text{TCa}^*] - (Z_1 + Y_2) [\text{TCa}]$$

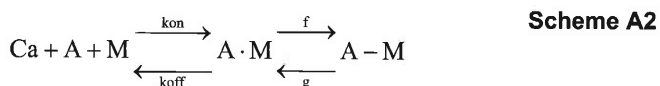
$$d[\text{TCa}^*]/dt = Y_2 [\text{TCa}] + Z_3 [\text{T}^*] - (Z_2 + Y_3 + Y_d) [\text{TCa}^*]$$

$$d[\text{T}^*]/dt = Y_3 [\text{TCa}^*] - (Z_3 + Y_4 + Y_d) [\text{T}^*]$$

$$[\text{T}] = 1 - [\text{TCa}] - [\text{TCa}^*] - [\text{T}^*]$$

The Ca bound to troponin is given by  $([\text{TCa}] + [\text{TCa}^*]) \times [\text{troponin}]_{\text{total}}$ , with  $[\text{troponin}]_{\text{total}} = 0.07$  mM.

The stoichiometry for  $\text{Ca}^{2+}$  binding to troponin is one to one, and thus only a slight positive cooperativity is found in the steady-state relationship between  $[\text{Ca}^{2+}]$  and  $[\text{TCa}^*]$  ( $n_H = 1.27$ ). The three-state cooperative model of Robinson *et al.* [4] reads



where A is the regulatory unit consisting of a troponin-actin complex and M the myosin head.  $\text{A} \cdot \text{M}$  and  $\text{A} - \text{M}$  represent the cross bridges with weak and strong binding, respectively. Although one-to-one stoichiometry is assumed for the  $\text{Ca}^{2+}$  binding to troponin, a high cooperativ-

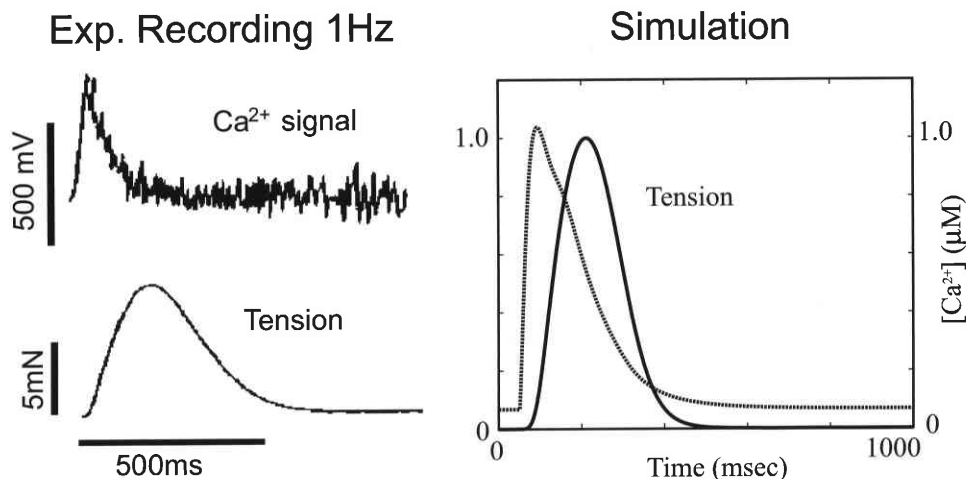


**Fig. A1.** Reconstruction of the developed tension. The left panel refers to Pieske *et al.* [13], and the right panel is the simulation result of isometric contraction induced by a  $\text{Ca}^{2+}$  transient shown as a dotted curve repeated with 1 Hz frequency.

ity of the Hill coefficient  $n_H > 5$  was observed in experiments [4, 12] and was reconstructed in the relationship between  $[\text{Ca}^{2+}]$ – $[\text{A-M}]$  by introducing nearest-neighbor cooperative influences. In detail, the  $\text{Ca}^{2+}$  dissociation rate from regulatory units ( $k_{\text{off}}$ ) and the cross-bridge dissociation rate ( $g$ ) decreases, though the cross-bridge association rate ( $f$ ) increases with progressive activation of the system. However, it is not possible to reconstruct the L-F relationship by using the Robinson model, simply because the length of sarcomere was not included in the model. For convenience in model development, we replaced  $Y_1$  and  $Z_1$  in the NL model by  $k_{\text{on}}$  and  $k_{\text{off}}$  of the Robinson model, respectively, and  $Y_2$  and  $Z_2$  by  $f$  and  $g$ , respectively. The cooperativity parameters,  $U$ ,  $V$ ,  $W$ ,  $X$ , and  $Z$  in the original paper were used with no modification.

$$Y_1 \text{ (ms}^{-1}\text{)} = a_{\text{cm}} [\text{Ca}^{2+}] \quad (\text{A1})$$

$$Z_1 \text{ (ms}^{-1}\text{)} = b_{\text{cm}} (1 + f_{23} (e^{-2.09} - 1))^2 (1 + f_3 (e^{0.73} - 1))^2 \quad (\text{A2})$$

$$Y_2 \text{ (ms}^{-1}\text{)} = f_{\text{cm}} (1 + f_{23} (e^{2.96} - 1))^2 (1 + f_3 (e^{-2.1} - 1))^2 \quad (\text{A3})$$

$$Z_2 \text{ (ms}^{-1}\text{)} = g_{\text{cm}} (1 + f_3 (e^{-0.26} - 1))^2 \quad (\text{A4})$$

$$Y_3 = Z_1 \quad (\text{A5})$$

$$Z_3 = 40 \cdot Y_1 \quad (\text{A6})$$

$$Y_4 \text{ (ms}^{-1}\text{)} = 0.24 \quad (\text{A7})$$

$$Y_d \text{ (}\mu\text{m}^{-2}\cdot\text{ms)} = 9000 (dX/dt)^2,$$

or

$$Y_d \text{ (}\mu\text{m}^{-2}\cdot\text{ms)} = 180 (dX/dt)^2 \text{ when } dX/dt > 0. \quad (\text{A8})$$

After model fitting to the experimental recordings, other parameters were set as follows. The original kinetic rates for the skeletal muscle for  $\text{Ca}^{2+}$  association ( $k_{\text{on}} = 17.3 \text{ mM}^{-1}\cdot\text{ms}^{-1}$ ) and dissociation ( $k_{\text{off}} = 0.2 \text{ ms}^{-1}$ ), cross-

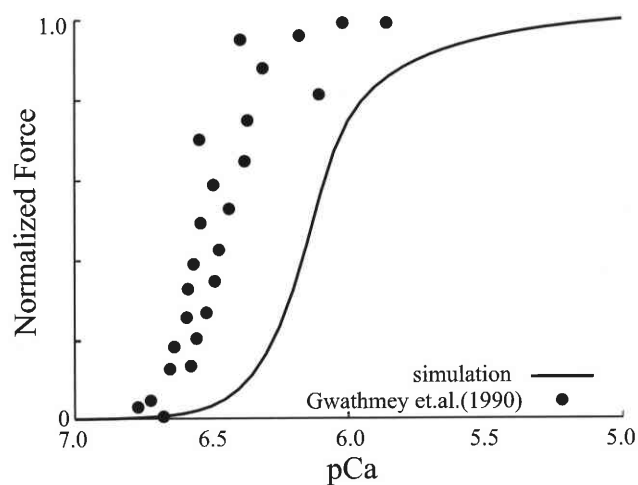


**Fig. A2.** Reconstruction of the  $\text{pCa}^{2+}$ -force relationship. The crosses represent the experimental data obtained by Gwathmey and Hajjar [14], and the continuous curve is the simulation result of the hybrid model.  $n_H = 3.41$  and the half maximum  $\text{pCa}_{0.5} = 6.11$  in the simulation.

bridge attachment ( $f = 0.00136 \text{ ms}^{-1}$ ) and detachment ( $g = 0.015 \text{ ms}^{-1}$ ), were adjusted for the cardiac muscle as represented in  $a_{\text{cm}}$ ,  $b_{\text{cm}}$ ,  $f_{\text{cm}}$ , and  $g_{\text{cm}}$  in Eqs. A9–A12 to reconstruct an average time course of developed tension as recorded, using human heart trabeculae as shown in Fig. A1 [13].

$$a_{\text{cm}} \text{ (mM}^{-1}\cdot\text{ms}^{-1}\text{)} = 32 \quad (\text{A9})$$

$$b_{\text{cm}} \text{ (ms}^{-1}\text{)} = 0.054 \quad (\text{A10})$$

$$f_{\text{cm}} \text{ (ms}^{-1}\text{)} = 0.0000851 \quad (\text{A11})$$

$$g_{\text{cm}} \text{ (ms}^{-1}\text{)} = 0.000649 \quad (\text{A12})$$

According to the  $\text{Ca}^{2+}$  sensitivity in intact myocytes, which is higher than in skinned fiber, the  $[\text{Ca}^{2+}]$ -force curve in the Robinson model [4] was shifted to the left by decreasing the dissociation rate  $k_{\text{off}}$  ( $b_{\text{cm}} = 0.054 \text{ ms}^{-1}$ ) in the hybrid model (Fig. A2). In the original Robinson model the half-saturation concentration  $K_{0.5}$  equals approxi-

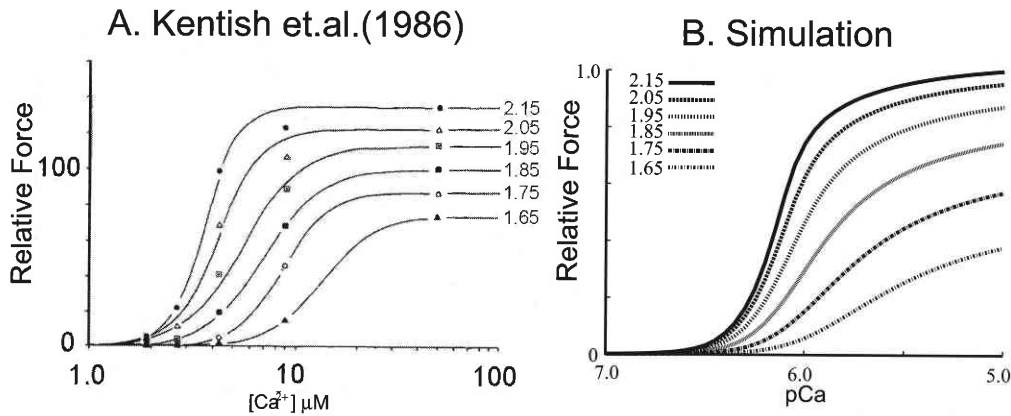


**Fig. A3.** The Ca<sup>2+</sup>-force relations at various sarcomere lengths (SL). The experimental data by Kentish *et al.* [12] is cited for a comparison with the simulation results in the right panel. Note that the decrease in the slope with decreasing SL is well simulated.

mately 2 μM, whereas in the presented model it is approximately 0.7 μM. This value is higher than the original measurement in the human trabeculae of ~0.56 μM [14]. However, to avoid a significant amount of remaining  $F_b$  at the end of diastole, a shift of the  $F_b$ -[Ca<sup>2+</sup>] relation was necessary in the present study, as shown in Fig. A2.

To be consistent with the Robinson model,  $Y_3$  was set equal to  $Z_1$ , and  $Z_3$  was 40  $Y_1$  according to the NL model. To achieve a slower time course in the cardiac muscle compared to the skeletal muscle, the constants of  $f_{cm}$ , and  $g_{cm}$  were much reduced from the original values, whereas the rate  $Y_d$  was left as it is in the original NL model to maintain the rapid recovery of force after an instantaneous shortening of the fiber.

In the NL model, the dependence of developed tension on the sarcomere length is well reconstructed simply by assuming an effective concentration of [TCa] ([TCa]<sub>eff</sub> in Negroni and Lascano [3]) for the cross-bridge attachment, but in the Robinson model the L-F relation was not considered at all. Recently, Schneider *et al.* [15] simulated the sarcomere length-dependent force generation (Frank-Starling law) successfully by introducing the titin's passive tension. In their model, the cross-bridge concentration was altered by introducing the SL-dependent rate of the myosin binding through titin-based passive tension. We introduced this relation simply by replacing the fractional activation parameters  $\eta$  and  $\varepsilon$  by new parameters  $f_{23}$  (Eq. A13) and  $f_3$  (Eq. A14), respectively, only for the sake of computational simplicity.

$$f_{23} = S \cdot ([TCa] + [TCa^*] + [T^*]) \quad (A13)$$

$$f_3 = S \cdot ([TCa^*] + [T^*]) \quad (A14)$$

with  $0 \leq [TCa], [TCa^*], [T^*] < 1.0$ ,

$$S = \frac{1}{\left(1 + e^{-\frac{L-0.85}{-0.08}}\right) \left(1 + e^{\frac{L-1.4}{0.06}}\right)} \quad (A15)$$

The  $f_{23}$  and  $f_3$  are described using an “S function” given by Eq. A15, where  $L$  (μm) represents the half-sarcomere length in the original NL model. The new equations A13, A14, and A15 well reconstructed the force-pCa<sup>2+</sup> rela-

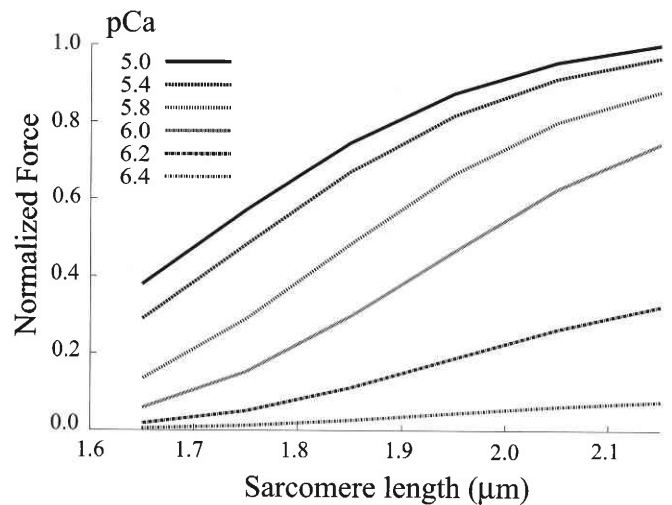


**Fig. A4.** Reconstruction of the length-force relations at different [Ca<sup>2+</sup>] using the hybrid model.

tions [12] measured at different sarcomere lengths in Fig. A3 and the force-sarcomere length relations at different [Ca<sup>2+</sup>] in Fig. A4.

As demonstrated in the single fiber experiment in skeletal muscle [1], the velocity of the filament sliding during isotonic contraction decreases in an exponential manner as the mechanical load is decreased. In the NL model, however, the F-V relation is linear (Eq. A16).

$$dX/dt \text{ (}\mu\text{m}\cdot\text{ms}^{-1}\text{)} = 1.2 \cdot (h - h_c) \text{ with } h_c = 0.005 \mu\text{m} \quad (A16)$$

In contrast, the original data points for initial rapid shortening in the skeletal muscle obtained in Piazzesi *et al.* [1] could be fitted with an equation,

$$dX/dt \text{ (}\mu\text{m}\cdot\text{ms}^{-1}\text{)} = B_{\text{eff}} \left( e^{\frac{h_c - h}{0.00225}} - 1 \right) \quad (A17)$$

with  $B_{\text{eff}} = 1.887 \mu\text{m/ms}$ .

We used Eq. A17 to calculate the sliding rate of the myosin head in the present cardiac cell model because it overlaps fortuitously with Eq. A16 over a physiological range from 0.6 to 1.0  $h_c$  (see Fig. 4 in RESULTS).

The myofilament force  $F_b$  is calculated as

$$F_b = A \cdot S \cdot ([TCa^*] + [T^*]) \cdot h \quad (A18)$$

with  $A = 1,800$  and  $450 \text{ mN/mm}^2/\mu\text{m}/\mu\text{M}$  in the ventricle [3] and atrium [16], respectively.

For calculating the force of the parallel elastic component,  $F_p$ , we used the format of  $F_p$ , as used by Landesberg and Sideman [17].

$$F_p = \begin{cases} K_{PE}(e^{D \cdot (L/L_0 - 1)} - 1) & \text{if } L \geq L_0 \\ -K_{PL}(1 - L/L_0) & \text{if } L < L_0 \end{cases} \quad (A19)$$

with  $K_{PE} = 3 \text{ mN/mm}^2$ ,  $K_{PL} = 30 \text{ mN/mm}^2$ ,  $D = 10$ , and  $L_0 = 0.97 \mu\text{m}$  (model fit) for both the ventricle and atrium.

We thank Dr. Yu Shimizu (Ito) for constructive comments on the manuscript. This study was supported by the Leading Project for Biosimulation of the Ministry of Education, Culture, Sports, Science and Technology of Japan.

REFERENCES

1. Piazzesi G, Lucii L, Lombardi V. The size and the speed of the working stroke of muscle myosin and its dependence on the force. *J Physiol.* 2002;545:145-51.
2. Negroni JA, Lascano EC. Concentration and elongation of attached cross-bridges as pressure determinants in a ventricular model. *J Mol Cell Cardiol* 1999;31:1509-26.
3. Negroni JA, Lascano EC. A cardiac muscle model relating sarcomere dynamics to calcium kinetics. *J Mol Cell Cardiol.* 1996;28:915-29.
4. Robinson JM, Wang Y, Glenn W, Kerrick L, Kawai R, Cheung HC. Activation of striated muscle: nearest-neighbor regulatory-unit and cross-bridge influence on myofilament kinetics. *J Mol Biol.* 2002;322:1065-88.
5. ten Tusscher KHW, Noble D, Noble PJ, Panfilov AV. A model for human ventricular tissue. *Am J Physiol Heart Circ Physiol.* 2004;286:H1573-89.

6. Shim EB, Leem CH, Abe Y, Noma A. A new multi-scale simulation model of the circulation: from cells to system. *Philos Transact A Math Phys Eng Sci.* 2006;364:1483-500.
7. Gaasch WH, Battle WE, Oboler AA, Banas J, Levine HJ. Left ventricular stress and compliance in man. With special reference to normalized ventricular function curves. *Circulation.* 1972;45:746-62.
8. Nygren A, Fiset C, Firek L, Clark JW, Lindblad DS, Clark RB, Giles WR. Mathematical model of an adult human atrial cell: the role of K<sup>+</sup> currents in repolarization. *Circ Res.* 1998;82:63-81.
9. Frank O. Zur Dynamik des Herzmuskels. *Z Biol.* 1895;32:370-447.
10. Katz AM. Ernest Henry Starling, his predecessors, and the "Law of the Heart" *Circulation.* 2002;106:2986-92.
11. Huxley AF, Simmons RM. Proposed mechanism of force generation in striated muscle. *Nature* 1971;233:533-8.
12. Kentish JC, Ter Keurs HE, Ricciardi L, Bucx JJ, Noble MI. Comparison between the sarcomere length-force relations of intact and skinned trabeculae from rat right ventricle. influence of calcium concentrations on these relations. *Circ Res.* 1986;58:755-68.
13. Pieske B, Sutterlin M, Schmidt-Schweda S, Minami K, Meyer M, Olschewski M, Holubarsch C, Just H, Hasenfuss G. Diminished post-rest potentiation of contractile force in human dilated cardiomyopathy. Functional evidence for alterations in intracellular Ca<sup>2+</sup> handling. *J Clin Invest.* 1996;98:764-76.
14. Gwathmey JK, Hajjar RJ. Effect of protein kinase C activation on sarcoplasmic reticulum function and apparent myofibrillar Ca<sup>2+</sup> sensitivity in intact and skinned muscles from normal and diseased human myocardium. *Circ Res.* 1990;67:744-52.
15. Schneider NS, Shimayoshi T, Amano A, Matsuda, T. Mechanism of the Frank-Starling law—a simulation study with a novel cardiac muscle contraction model that includes titin and troponin I. *J Mol Cell Cardiol.* 2006;41:522-36.
16. Beyar R, Sideman S. Atrioventricular interactions: a theoretical simulation study. *Am J Physiol.* 1987;252:H653-65.
17. Landesberg A, Sideman A. Mechanical regulation of cardiac muscle by coupling calcium kinetics with cross-bridge cycling: a dynamic model. *Am J Physiol.* 1994;267:H779-95.
18. Heldt T, Shim EB, Kamm RD, Mark RG. Computational modeling of cardiovascular response to orthostatic stress. *J Appl Physiol.* 2002;92:1239-54.
19. Ursino M. Interaction between carotid baroregulation and the pulsating heart: a mathematical model. *Am. J. Physiol.* 1998;275:H1733-47.